International Journal of Heat and Mass Transfer 52 (2009) 735–743

Contents lists available at ScienceDirect

International Journal of Heat and Mass Transfer

journal homepage: www.elsevier.com/locate/ijhmt

Transport properties of liquid argon in krypton nanochannels: Anisotropy and non-homogeneity introduced by the solid walls

F. Sofos, T. Karakasidis *, A. Liakopoulos

Hydromechanics and Environmental Engineering Laboratory, School of Engineering, University of Thessaly, 38834 Pedion Areos, Volos, Greece

ARTICLE INFO

Article history:
Received 21 December 2007
Available online 9 September 2008

Keywords:
NEMD simulation
Nanofluid dynamics
Nanoscale phenomena
Transport properties
Non-continuum effects

ABSTRACT

In this work we calculate the transport properties of liquid argon flowing through a nanochannel formed by krypton walls. Non-equilibrium molecular dynamics (NEMD) simulations are performed assuming flow conditions corresponding to the macroscopic equivalent of planar Poiseuille flow. We examine the effect of channel width and system temperature on diffusion coefficient, shear viscosity and thermal conductivity. The results show clearly the existence of a critical width, in the range 7–18σ, below which the behavior of transport properties is affected in comparison to bulk properties. In fact for small width values, diffusion coefficient is highly anisotropic, the component normal to the wall being the smaller one. For the same width range, diffusivities along all directions are higher in the central layers than those close to the walls. Similarly, shear viscosity increases for small channel width values while thermal conductivity decreases. All properties approach bulk values as the channel width increases. The layers close to the walls always present distinctly different behavior due to the interaction with the wall atoms. The observed behavior is of particular importance in the design of nanofluidic devices.

1. Introduction

Micro and nanofluidic simulations have attracted considerable attention recently, due to the growing interest for nanosystems in many technological and scientific fields. Experimental studies at the atomic scale are difficult to perform and, thus, atomistic simulation techniques provide the means for exploring regions (either in physical space or in parameter space) that cannot be accessed by experiment. Consequently, molecular computer simulations have established themselves as a valuable alternative to theoretical and experimental work. In addition to its role in interpreting experimental results, molecular computer simulation is vital in determining physical properties of materials as well as in exploratory research [1].

Among computer simulation techniques, equilibrium molecular dynamics (EMD) has been extensively used for the calculation of transport properties of fluids in equilibrium. For atomic systems far from equilibrium, such as liquid flows in channels, non-equilibrium molecular dynamics (NEMD) offers an effective flow simulation method as well as an alternative method for the calculation of transport properties of liquids, either in simple monoatomic fluids [2–9] or in more complex fluids [10–12]. Among the transport properties, diffusion coefficient, shear viscosity and thermal conductivity have attracted most of the interest of the scientific community as they control the rates of mass, momentum and energy transport.

Diffusivity issues concerning liquid flows at nanoscale have been addressed by many researchers. Bitsanis et al. [13] studied fluid argon both in equilibrium and in Couette flow and concluded that diffusivity is not affected by the presence of flow in the system. Murad et al. [14] studied confined fluids in slit, tubular and cubic pores and found that diffusion coefficient values are not systematically affected by the size of the channels studied for channel width, h, in the range $h = 6\sigma$–10σ, where σ is the LJ-potential length scale. A useful review on diffusivity issues in slit pores in [3] shows that mobility is maintained even in pore widths of 2.0σ, while diffusion parallel to the pore wall below $h = 4.0\sigma$ becomes an oscillating function of the channel width. Beyond 4.0σ, diffusivity increases smoothly and it reaches the bulk value at 11.57σ.

Shear viscosity is another transport property of fluids that has attracted considerable interest among researchers. A number of computational studies of shear viscosity by EMD or NEMD have been reported in the literature. In the area of nanofluidics, Bitsanis et al. [15] found that shear viscosity in Poiseuille flow is indistinguishable from the homogenous fluid viscosity down to channel widths of 6–7σ, while, below 4σ, viscosity vs. channel width becomes an oscillating function. Hu et al. [16] found that the viscosity of a confined lubricant increases as the channel width decreases.

EMD or NEMD calculation of thermal conductivity in nanochannels is of particular interest, too. Evans [17], in his early work on thermal conductivity of argon in a confined system, found that this

* Corresponding author. Tel.: +30 2421074163; fax: +30 2421074169.
E-mail address: thkarak@uth.gr (T. Karakasidis).

0017-9310/$ - see front matter © 2008 Elsevier Ltd. All rights reserved.
doi:10.1016/j.ijheatmasstransfer.2008.07.022

Nomenclature

L_x	Length of the computational domain in the x-direction
L_y	Length of the computational domain in the y-direction
L_z	Length of the computational domain in the z-direction
h	Channel width
V	Volume of the computational domain ($L_x \times L_y \times L_z$)
T	Temperature
N	Number of atoms
K	Spring constant
$\mathbf{r}_i$	Position vector of atom i
$\mathbf{r}_{ij}$	Distance vector between ith and jth atom
r_{eq}	Position of a wall atom on fcc lattice site
F_{ext}	External driving force (magnitude)
k_B	Boltzman constant
m	Argon atom mass
D	Diffusion coefficient, $D = \frac{D_x + D_y + D_z}{3}$
D_{lay}	Diffusion coefficient value in a specific layer along the channel
MSD	Mean square displacement
v^i	ith component of atomic velocity, i = 1,2,3
$u(\mathbf{r}_{ij})$	LJ potential of atom i with atom j
$\mathbf{J}_p$	Microscopic stress tensor
$\mathbf{J}_q$	Microscopic heat flow
$\mathbf{v}_i$	Velocity vector of atom i
$\mathbf{I}$	Unitary tensor

Greek symbols

σ	Length parameter in the LJ potential
ε	Energy parameter in the LJ potential
ρ^*	Reduced density
η_s	Shear viscosity
λ	Thermal conductivity

quantity is linearly dependent to the external field applied to drive the flow. Murad et al. [18] showed that the vertical to the walls component of thermal conductivity is affected by the value of the elastic spring constant of the channel walls; its value decreases as this constant increases. Liu et al. [19] calculated thermal conductivity for thin argon films with Fourier's law and found that thermal conductivity increases as the film thickness increases, until it reaches the bulk value at 100 nm. Yonetani and Kinugawa [20] compared calculated values on thermal conductivity with experimental measurements of liquid para-hydrogen and found that it increases as temperature rises.

In nanochannels of width below 6σ, the above transport properties have not been thoroughly studied with NEMD as far as we know. Wall-fluid interactions play a crucial role in the behavior of flow properties in channels of small width, especially in the range $h = 2.65\sigma$–18.58σ [21]. The no-slip condition at the wall and the parabolic behavior of the velocity profile, expected from the continuum theory, break down in channels of small width and density profiles reveal strong ordering of the fluid. Thus, it is expected that the calculation of transport properties in small confined systems, especially at layers adjacent to the walls, will be of interest both from the fundamental point of view as well as for technological applications such as MEMS, lab-on-chip applications, nanomixers, etc.

When the width of the channel becomes very small, wall roughness becomes important. Roughness at the atomic scale can be classified as thermal, random or periodic [22]. Several molecular dynamics simulation works [22–27] examine mainly the effect of the roughness on the slip length. The results for simple fluids indicate that surface roughness can lead to slip near the solid boundary and affect fluid ordering [23–25]. For more complex fluids (water, hexadecane) the general trend observed is that the diffusion coefficient decreases near a rough wall [26] and viscosity is increased [27]. In our work we have assumed atomically flat wall surfaces so that only thermal roughness affects our transport property results.

In this work we study the transport properties of liquid argon by non-equilibrium molecular dynamics (NEMD) simulation of Poiseuille flow between two "infinite" krypton walls. We report on calculated values of the diffusion coefficient, D, shear viscosity, η_s and thermal conductivity, λ, for channel widths in the range 2.65σ–18.58σ and system temperature from 100 to 150 K. All transport properties are calculated both in distinct layers parallel to the channel walls as well as average values over the whole computational domain.

This paper is organized as follows. In Section 2 the molecular system modeled is described. The basis for the calculation of three transport properties (D, η_s, λ) is briefly presented in Section 3. Results are shown and discussed in Section 4, and concluding remarks are presented in Section 5.

2. System modeling

The NEMD technique is used to simulate planar Poiseuille flow of liquid argon. The geometry of the system under examination is presented schematically in Fig. 1. The walls consist of two layers of krypton atoms arranged on fcc lattice. Atomic interactions are described by a Lennard–Jones 12–6 potential:

$$v^{LJ}(r_{ij}) = 4\varepsilon((\sigma/r_{ij})^{12} - (\sigma/r_{ij})^{6}) \quad (1)$$

where the parameters of the Lennard–Jones potential are: $\sigma_{Ar-Ar} = 0.3405$ nm, $\sigma_{Kr-Kr} = 0.3633$ nm, $\sigma_{Ar-Kr} = 0.3519$ nm, $\varepsilon_{Ar-Ar}/k_B = 119.8$ K, $\varepsilon_{Kr-Kr}/k_B = 167.0$ K, $\varepsilon_{Ar-Kr}/k_B = 141.4$ K, the cut-off radius is $r_c = 2.5\sigma$, the atomic mass of argon is $m_{Ar} = 39.95$ a.u. and the atomic mass of krypton is $m_{Kr} = 83.8$ a.u.

Flows in several nanochannels of variable width (h) have been simulated (see Table 1). The average fluid density $\rho^* = 0.642$ (in units of σ^{-3}) has been kept constant. The streamwise and spanwise dimensions L_x and L_y as well as the number of wall atoms are kept constant throughout this work ($L_x = L_y = 36.15$ Å, $N_{Kr} = 288$). Periodic boundary conditions are assumed in the x- and y-direction.

Wall atoms are kept around their original fcc lattice positions due to an elastic spring potential $u_{wall}(|\mathbf{r}(t) - \mathbf{r}_{eq}|) = \frac{1}{2}K(|\mathbf{r}(t) - \mathbf{r}_{eq}|)^2$, where $\mathbf{r}(t)$ is the position of an atom at time t, $\mathbf{r}_{eq}$ is its initial lattice position and K is the spring constant. As explained in [28], if we compute the second derivative of this potential and the second derivative of the LJ potential (Eq. (1)), evaluate

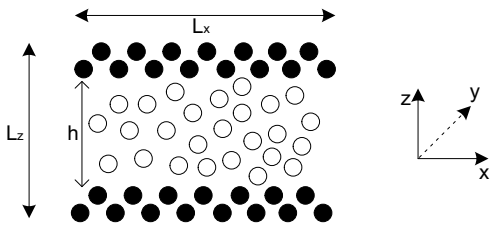

Fig. 1. The atomic system under examination.

Table 1
Dimensions of the systems under examination

Case	L_z (Å)	h (Å)	h/σ	Fluid atoms
1	18.08	9.04	2.65	192
2	24.10	15.06	4.42	320
3	36.15	27.11	7.9	576
4	72.30	63.26	18.58	1344

both derivatives at $r = r_0 = 2^{1/6}\sigma$, and equate the results, we get $K = 57.15\varepsilon/\sigma^2$. We remind the reader that $r_0 = 2^{1/6}\sigma$ is the distance where the LJ potential reaches its minimum. The value of $K = 57.15\ \varepsilon/\sigma^2$ was used in all our simulations.

An external driving force F_{ext} is applied along the x direction to every fluid particle during the simulation. The magnitude of the external applied force is selected in order to avoid non-linear variations in fluid temperature induced by the flow [4] and is equal to 1.8075 pN. The wall atoms absorb the increase in kinetic energy of the fluid atoms and Nosé–Hoover thermostats at the thermal walls are employed in order to keep the system's temperature constant. A detailed description of the use of Nosé–Hoover thermostats is provided in references [29] and [30]. We use two independent thermostats one for the upper wall and another for the lower wall in order to achieve better thermalisation of the wall atoms.

The simulation step is 10^{-2} ps. In the beginning of a simulation run fluid atoms are located on fcc sites. Atoms are assigned appropriate random initial velocities in order to reach the desired temperature. The system reaches equilibrium state after a run of 10^5 timesteps (NVE). Then, NEMD simulations are performed with a duration of 10^5 timesteps.

3. Theoretical relations

The diffusion coefficient can be obtained using either the Einstein's relation

$$D = \lim_{t\to\infty} \frac{1}{2dNt}\left\langle \sum_{j=1}^{N} [\mathbf{r}_j(t) - \mathbf{r}_j(0)]^2 \right\rangle \tag{2}$$

or Green–Kubo's relation

$$D = \frac{1}{3N}\int_0^\infty \left\langle \sum_{j=1}^{N} \mathbf{v}_j(0)\cdot\mathbf{v}_j(t) \right\rangle \tag{3}$$

where $\mathbf{r}_j$ is the position vector of the jth atom and d is the dimensionality of the system ($d = 1$ for diffusivity calculation in one direction, $d = 2$ in two directions and $d = 3$ in three directions) and $\mathbf{v}_j$ is the velocity vector of the jth atom.

The two relations are equivalent and provide the same results [2,3]. Relations 2 and 3 are derived for systems in equilibrium, but they can be used for non-equilibrium systems as well, provided one excludes the drift contribution from the flow [3]. In the present work we have used Einstein's relation for the calculation of the diffusion coefficient. The computation is carried out in two steps. In the first step the Mean Square Displacement (*MSD*) is obtained from the definition

$$MSD(t) = \frac{1}{N}\left\langle \sum_{j=1}^{N} [\mathbf{r}_j(t) - \mathbf{r}_j(0)]^2 \right\rangle \tag{4}$$

and subsequently D is evaluated based on Eq. (2) which can be written as

$$D = \lim_{t\to\infty} \frac{1}{2dt} MSD(t) \tag{5}$$

Shear viscosity and thermal conductivity for systems in equilibrium can be calculated using the Green–Kubo formalism, as described in [31]. These relations can be used without modification in NEMD as long as we stay in the linear regime close to equilibrium [32]. When the system is not in equilibrium, due to the existence of an external force, the magnitude of the external force should be small enough for linearization to hold [4,33]. Our system is in the linear regime for all channel widths studied when $F_{ext} = 1.8075$ pN.

Shear viscosity η_s for a pure fluid is computed by the relation

$$\eta_s = \frac{1}{Vk_BT}\int_0^\infty dt \langle J_p^{xy}(t)\cdot J_p^{xy}(0)\rangle \tag{6}$$

where J_p^{xy} is the off-diagonal component of the microscopic stress tensor

$$J_p^{xy} = \sum_{i=1}^{N} m_i v_i^x v_i^y - \sum_{i=1}^{N}\sum_{j>1}^{N} r_{ij}^x \frac{\partial u(r_{ij})}{\partial r_{ij}^y} \tag{7}$$

$u(r_{ij})$ is the LJ potential of atom i interacting with atom j, r_{ij} is the distance between atoms i and j, and v_i^j is the j-component (j = x, y or z) of the velocity of atom i.

On the other hand, thermal conductivity λ can be calculated by the integration of the time-autocorrelation function of the elements of the microscopic heat flow J_q^x, i.e.,

$$\lambda = \frac{1}{Vk_BT^2}\int_0^\infty dt \langle J_q^x(t)\cdot J_q^x(0)\rangle \tag{8}$$

where the microscopic heat flow $\mathbf{J}_q$ is given by

$$\mathbf{J}_q = \frac{1}{2}\sum_{i=1}^{N} m_i(v_i)^2 v_i - \sum_{i=1}^{N}\sum_{j>1}^{N}\left[\mathbf{r}_{ij}:\frac{\partial u(r_{ij})}{\partial \mathbf{r}_{ij}} - \mathbf{I}\cdot u(r_{ij})\right]\cdot v_i \tag{9}$$

where $\mathbf{v}_i$ is the velocity vector of atom i and $\mathbf{I}$ is the unitary matrix.

4. Results and discussion

All transport properties are computed both in distinct layers and as total average values for the channel. The number of layers used in the computation varies and depends on the width of the channel. Specifically, two layers are considered in the channel of width $h = 2.65\sigma$, three layers for $h = 4.42\sigma$, four layers for $h = 7.9\sigma$ and five layers for $h = 18.58\sigma$, as shown in Fig. 2.

4.1. Diffusion coefficient

In Fig. 3a–c, we present the *MSD* diagrams in the streamwise direction (x-direction), the spanwise direction (y-direction) and the direction normal to the walls (z-direction) at 100, 120 and 150 K for $h = 2.65\sigma$ (*MSD* is presented in reduced units (MSD^*)). Diffusion coefficient values are extracted from *MSD* values according to Eq. (5). The diffusion coefficient in the z-direction has a rather small value and the Mean Square Displacement (*MSD*) diagram presents a small slope, meaning that fluid atoms are only slightly diffusing in the direction normal to the walls. The slope is significantly greater in the x- and y-directions.

Diffusion coefficient values were calculated for appropriately selected layers of equal width and the values are tabulated in Tables 2–5. At small channel widths ($h \lesssim 15\sigma$) local diffusion coefficient values in the z-direction ($D_{lay,z}$) are smaller than those in the x- and y-directions ($D_{lay,x}$, $D_{lay,y}$), which are practically the same. This is attributed to the fact that fluid atoms are strongly confined due to presence of the solid boundaries and, in the long term their diffusivity in the z-direction ($D_{lay,z}$) approaches zero value [3]. On the contrary, $D_{lay,x}$ and $D_{lay,y}$ are larger since the mobility of the fluid atoms is not inhibited by solid walls in these directions. However, as channel width increases ($h = 15\sigma$), $D_{lay,z}$ values approach $D_{lay,x}$ and $D_{lay,y}$ in all inner layers, except the two layers adjacent to the walls. This means that there is always strong anisotropy in

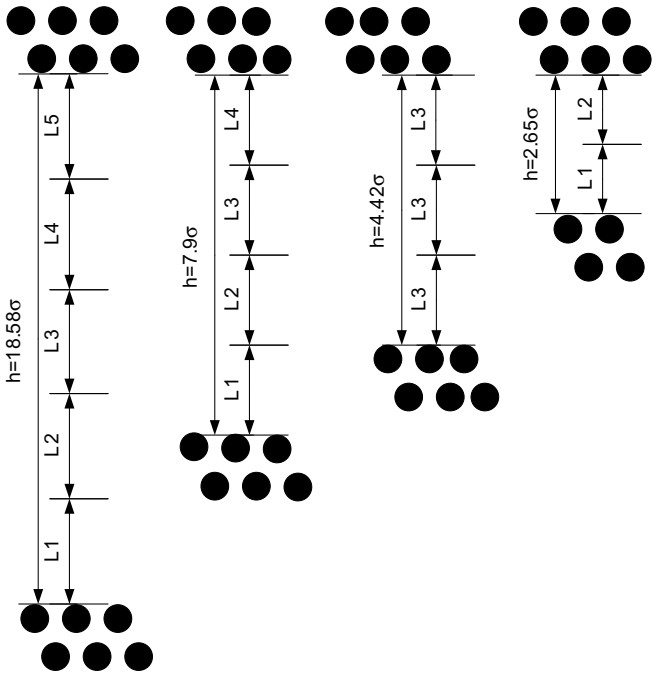

Fig. 2. Layer partitioning along each channel for the computation of transport properties.

diffusion coefficient in a layer of width about 1–1.5σ adjacent to the walls.

Comparing the values of the diffusion coefficient, we observe that all components of the diffusion coefficient are greater in the inner layers than they are at layers adjacent to the walls. This can be attributed to the fact that near the walls the repulsive solid/fluid effect is strong and fluid mobility in this region is small. At the inner layers, solid/fluid interaction is negligible, fluid atoms interact only with other identical fluid atoms (note that the fluid/fluid interaction potential is weaker than the solid/fluid) and their mobility is larger.

We also point out that the effect of system temperature is significant, since an increase in temperature from 100 to 120 K and, even more, to 150 K leads to a considerable rise in the respective diffusion coefficient values.

We turn now our attention back to the diffusion coefficient calculation based on the whole computational domain. It is of interest to summarize (Fig. 4) the calculated average channel diffusion coefficients D_x, D_y and D_z for all channels at 100, 120 and 150 K. In Fig. 4a, we observe that diffusion is isotropic along the x- and y- directions. In contradistinction, D_z has a smaller value for $h = 2.65\sigma$, but increases with a greater slope as the channel width increases. All diffusion coefficients converge to bulk value [34] at $h = 16\sigma$ and, furthermore, become isotropic. Similar behavior is observed for the other two system temperatures studied here (Fig. 4b and c). This behavior indicates the existence of a characteristic channel width ($h \approx 15\sigma$) below which the diffusion behavior is anisotropic.

In Fig. 5 we summarize the calculated average total channel diffusivity $D = \frac{D_x+D_y+D_z}{3}$ for all channels and temperatures studied. We can see that diffusivity is increasing as the channel width increases. One can explain the observed behavior if he takes into account the fact that at small channel widths the effect of walls on fluid atoms extends practically to the whole fluid range, resulting in an important modification of its behavior in comparison to the bulk where fluid atoms are embedded in the fluid environment. As the channel width increases, the percentage of fluid atoms that are out of the wall interaction increases and, thus, we approach bulk-like behavior. A similar behavior has been observed in an early work of

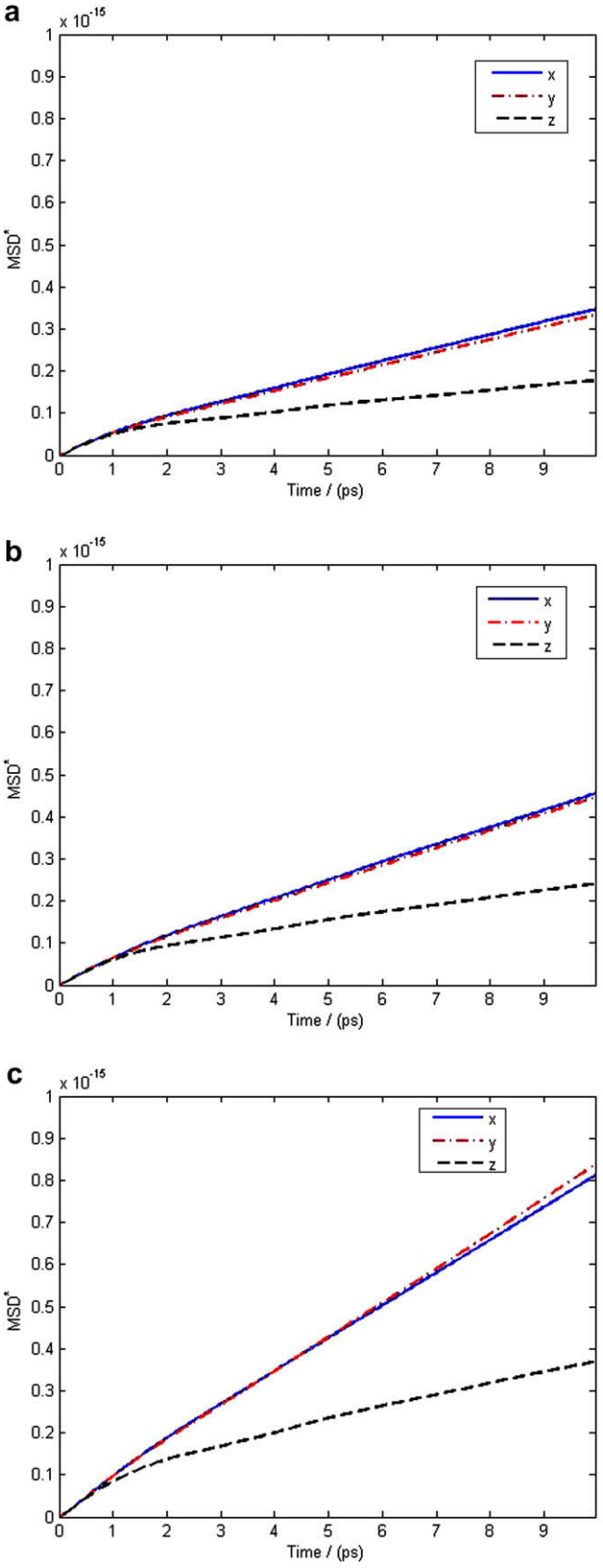

Fig. 3. Mean Square Displacement diagrams (in reduced units), in x-, y- and z-directions for 2.65σ-wide channel at (a) 100 K, (b) 120 K and (c) 150 K.

Table 2
Layer diffusion coefficient values, at x-, y- and z-directions ($D_{lay,x}$, $D_{lay,y}$ and $D_{lay,z}$, respectively), for a 2.65σ-wide channel at 100, 120 and 150 K and external driving force F_{ext} = 1.8075 pN

T/(K)	$10^5 \times D/(cm^2/s)$					
	$D_{lay,x}$		$D_{lay,y}$		$D_{lay,z}$	
	L1	L2	L1	L2	L1	L2
100	1.53	1.54	1.57	1.58	0.58	0.60
120	2.07	2.06	2.09	2.11	0.86	0.87
150	4.05	4.05	3.87	4.02	1.37	1.37

Table 3
As in Table 3, but for 4.42σ-wide channel

T/(K)	$10^5 \times D/(cm^2/s)$								
	$D_{lay,x}$			$D_{lay,y}$			$D_{lay,z}$		
	L1	L2	L3	L1	L2	L3	L1	L2	L3
100	1.59	2.93	1.61	1.56	3.06	1.57	1.18	1.92	1.16
120	2.47	3.86	2.43	2.44	3.93	2.49	1.68	2.43	1.68
150	3.89	5.40	3.77	3.83	5.45	3.85	2.58	3.21	2.60

Sommers and Davis [34], in a model of Couette flow in smooth and structured pores.

The results clearly indicate that diffusivities of a liquid may differ significantly from their known bulk values for nanochannels below a given characteristic dimension. This behavior should be taken into account in the design of nanofluidic devices, as well as in interpreting particle nanovelocimetry (nanoPIV) measurements close to solid surfaces [35].

4.2. Shear viscosity

Fig. 6a and b show shear viscosity integral diagrams, based on Eq. (6) and their respective autocorrelation functions (ACFs) across a 2.65σ-wide channel at 100, 120 and 150 K. The shear viscosity is calculated for layers L1 and L2, which are symmetrical with respect to the channel midplane. We present here results for layer L1 (computed values for L2 are the same within statistical errors). As we can see in Fig. 6a, the rise in temperature from 100 to 120 and 150 K results in a significant decrease in shear viscosity. The ACF diagram (see Fig. 6b) shows a fast decay to zero at 100 K right after the beginning of the simulation, at t = 0.5 ps. At T = 120 and 150 K, the decay is also fast in the beginning, but a slightly slower decay follows and ACF goes to zero at t = 0.75 ps. Note that the fast decay to zero for each temperature studied is an additional evidence of linearity for our system [36].

In Fig. 7a and b, shear viscosity integrals and ACFs for a 7.9σ-wide channel partitioned in four layers (L1–L4) at 120 K are presented. Shear viscosity is almost uniform across the channel and this fact reveals that solid/fluid interaction does not affect significantly the values of shear viscosity across the channel. ACFs in each channel layer converge to zero immediately after the beginning of the simulation. We obtain a similar uniform behavior for shear viscosity across the channel for h = 4.42 and 18.58σ (at T = 100 and 150 K).

We summarize the total average shear viscosity values as a function of channel width and system temperature in Fig. 8. One can see that for all temperatures at small channel width we have large values of shear viscosity and its value decreases as the channel width increases to attain the bulk value above 8σ. It can be seen that for higher system temperature the approach to bulk-like behavior is achieved faster. This behavior can be explained by the nature of shear viscosity which depends both on velocities and forces (Eqs. (6) and (7)). At small channel widths, the effect of different interactions of walls on fluid atoms extends nearly to the whole fluid and, as a result, we have an important modification of shear viscosity in comparison to bulk values. As the channel width increases, the percentage of fluid atoms that are out of the influence of wall increases resulting in a behavior close to the bulk. Increased temperature helps also overcome easier the effect of wall interactions. Thus, at higher temperature, approach to bulk-like behavior occurs faster.

It seems that the critical value of channel width in order to obtain bulk-like behavior for shear viscosity is similar to that in the case of diffusion coefficient, although it appears that is located rather at smaller values of h. The fact that shear viscosity is significantly larger compared to the bulk below a critical value is an important parameter that should be taken into consideration in the design of nanofluidic devices.

4.3. Thermal conductivity

Fig. 9a and b show thermal conductivity integrals and ACF diagrams across a 2.65σ-wide channel at 100, 120 and 150 K. Thermal conductivity is calculated for layers L1 and L2 (which are symmetrical with respect to the channel midplane). Here we present

Table 4
As in Table 3, but for 7.9σ-wide channel

T/(K)	$10^5 \times D/(cm^2/s)$											
	$D_{lay,x}$				$D_{lay,y}$				$D_{lay,z}$			
	L1	L2	L3	L4	L1	L2	L3	L4	L1	L2	L3	L4
100	2.31	4.19	4.24	2.27	2.21	4.31	4.33	2.17	1.80	3.62	3.68	1.77
120	3.36	5.10	5.15	3.33	3.35	5.43	5.37	3.41	2.47	4.42	4.46	2.53
150	4.91	6.83	6.86	4.94	5.03	7.29	7.04	4.88	3.53	5.95	5.90	3.42

Table 5
As in Table 3, but for 18.58σ-wide channel

T/(K)	$10^5 \times D/(cm^2/s)$														
	$D_{lay,x}$					$D_{lay,y}$					$D_{lay,z}$				
	L1	L2	L3	L4	L5	L1	L2	L3	L4	L5	L1	L2	L3	L4	L5
100	4.00	5.68	5.62	5.49	3.80	3.90	5.65	5.59	5.75	3.85	3.24	5.56	5.56	5.46	3.26
120	5.22	6.74	6.93	6.70	5.21	5.07	6.92	6.74	6.73	4.98	4.11	6.68	6.82	6.55	4.10
150	6.63	8.16	8.50	8.40	6.88	6.69	8.58	8.71	8.49	6.80	5.19	8.14	8.54	8.21	5.23

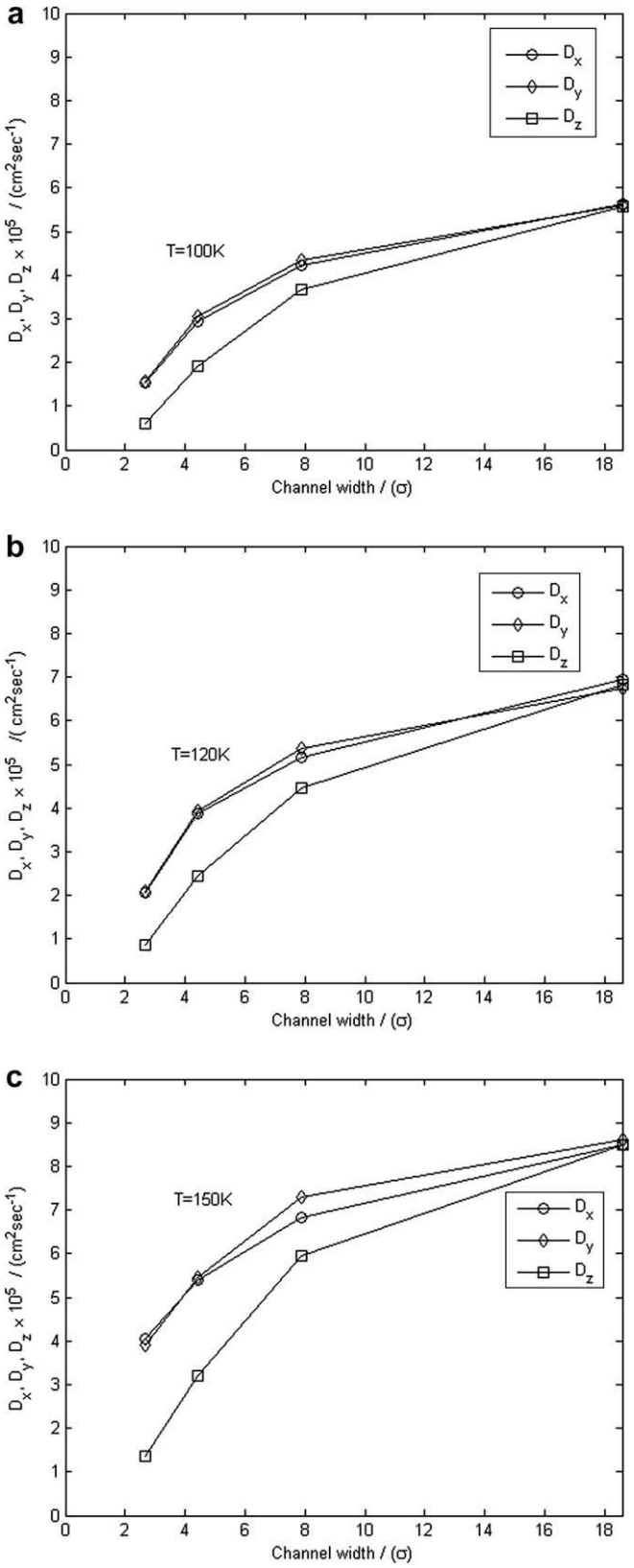

Fig. 4. Estimation of channel diffusion coefficient along the *x*-, *y*- and *z*-directions at (a) 100 K, (b) 120 K and (c) 150 K (lines are used only as a guide to the eye).

computed values for L1. It seems that as temperature rises from 100 to 120 and 150 K, thermal conductivity decreases slightly. The ACF diagrams decay to zero at $t = 1$ ps at 120 and 150 K. At

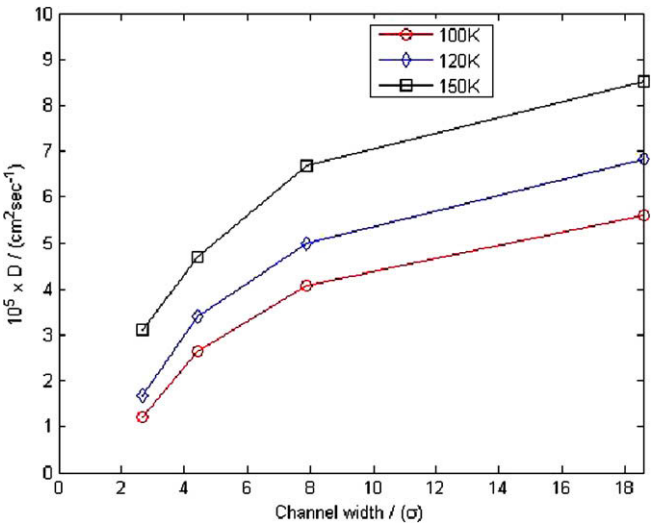

Fig. 5. Estimates of channel diffusion coefficient at 100, 120 and 150 K, for channel widths ranging from 2.65 to 18.58σ (lines are used only as a guide to the eye).

100 K, apart from the fast convergence to zero, we observe a fall below zero at $t = 0.5$ ps before ACF stabilizes to zero.

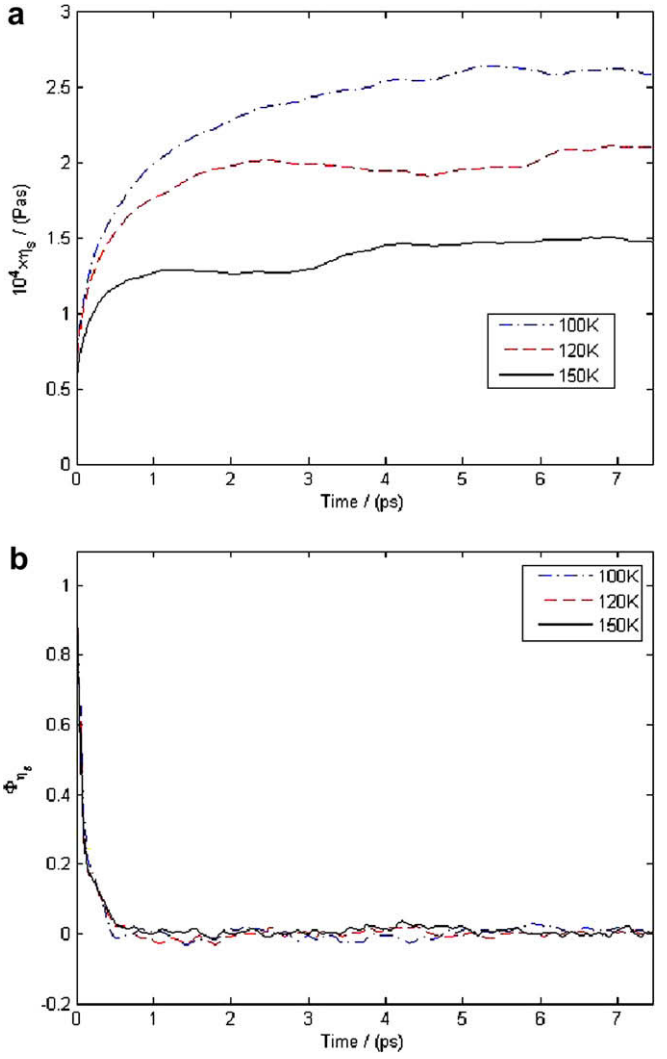

Fig. 6. Shear viscosity in layer L1 across a 2.65σ-wide channel in (a) integral diagram (b) ACF diagram.

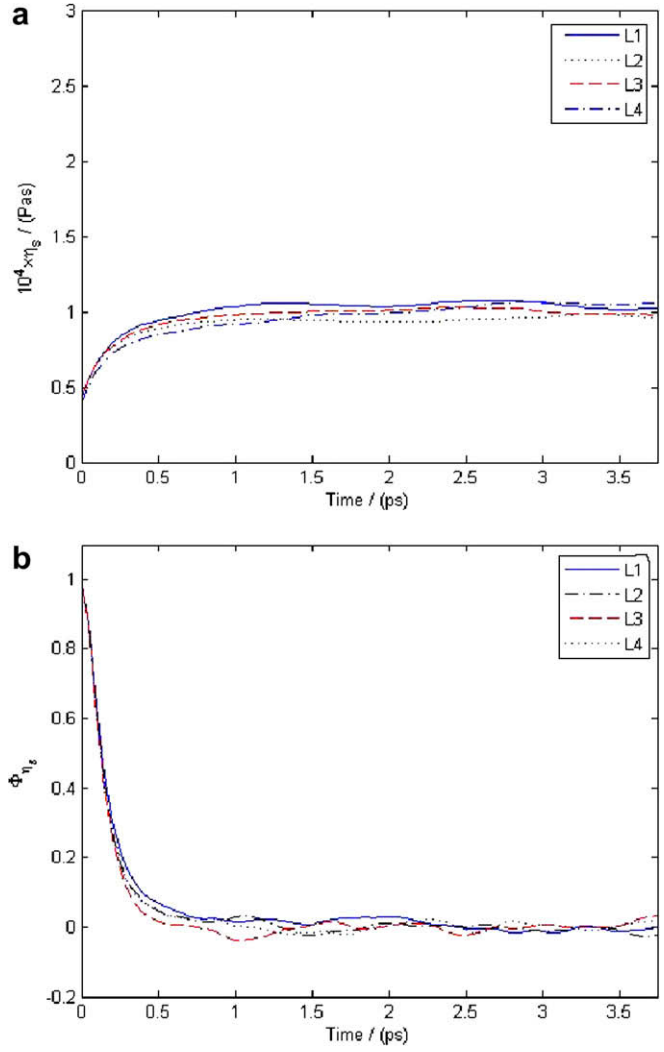

Fig. 7. Shear viscosity across a 7.9σ-wide channel at 120 K in (a) integral diagrams (b) ACF diagrams. L1 and L4 layers are adjacent to the walls, L2 and L3 layers are in the midplane of the channel.

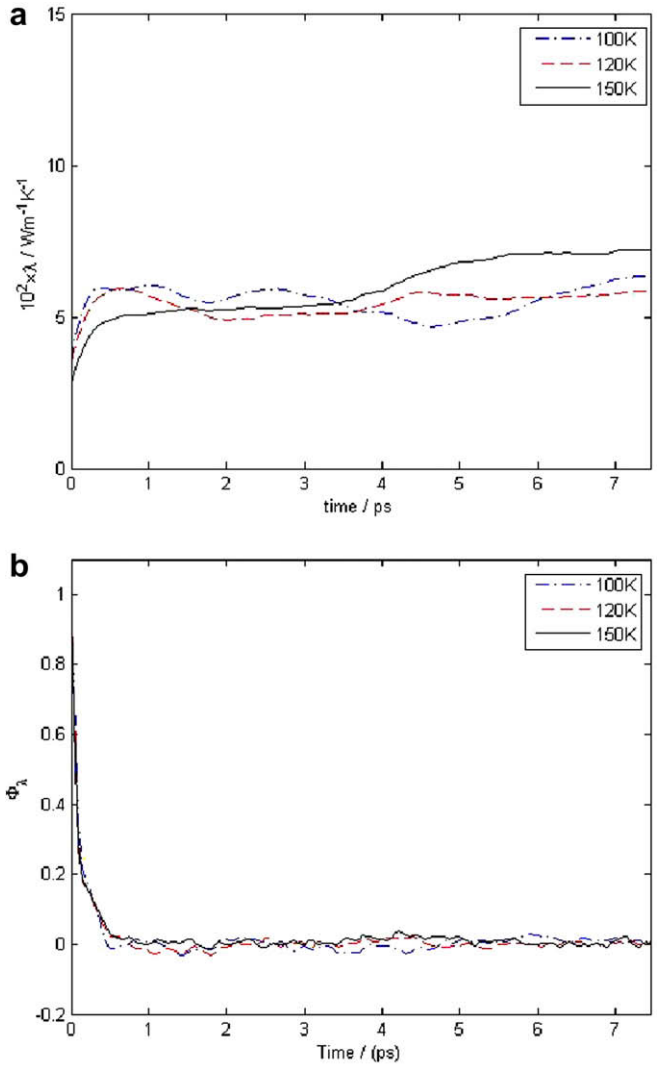

Fig. 9. Thermal conductivity in layer L1 across a 2.65σ-wide channel in a) integral diagram b) ACF diagram.

Thermal conductivity ACFs and integral diagrams calculated in four distinct layers (L1–L4) are shown in Fig. 11a and b. The channel here is 7.9σ-wide and the system temperature is 120 K. We observe that thermal conductivity is higher in the inner layers (L2, L3) compared to layers adjacent to the walls (L1, L4). All ACFs decay fast to zero as can be seen in Fig. 10b. We obtain a similar behavior for thermal conductivity across channels of width $h = 4.42$ and 18.58σ.

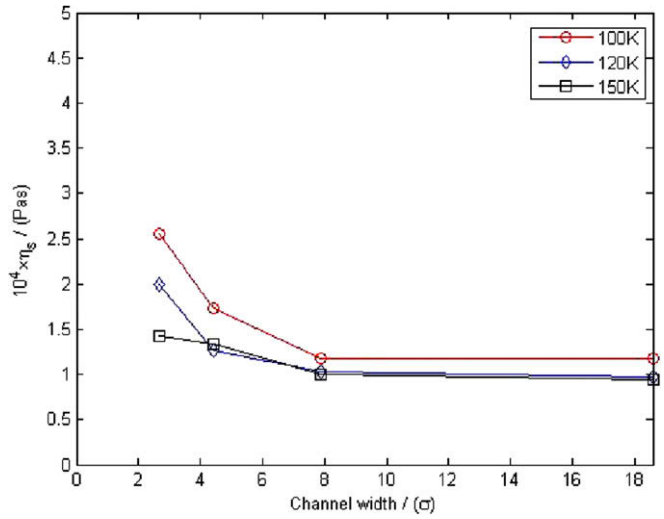

Fig. 8. Estimation of shear viscosity at 100, 120 and 150 K, for channel widths ranging from 2.65 to 18.58σ (lines are used only as a guide to the eye).

The calculated average thermal conductivity coefficients versus channel width for all system temperatures studied are summarized in Fig. 11. We observe that for all temperatures at small channel widths we have small values of thermal conductivity while λ increases as the channel width increases to attain the bulk value at about $h = 20\sigma$. However, we observe that at higher temperature thermal conductivity reaches its bulk value at smaller channel widths. This behavior can be understood on physical grounds, since thermal conductivity depends both on velocities and forces (Eqs. (8) and (9)). For small channel widths, the effect of walls on fluid atoms extends to nearly the whole range of fluid. As a result, it modifies the fluid behavior in comparison to the bulk. As the channel width increases, the percentage of fluid that is out of range of the wall interaction increases and, as a result, the fluid approaches bulk-like behavior. Increased temperature helps also overcome earlier the effect of wall interactions, thus, at higher temperature we approach bulk-like behavior faster.

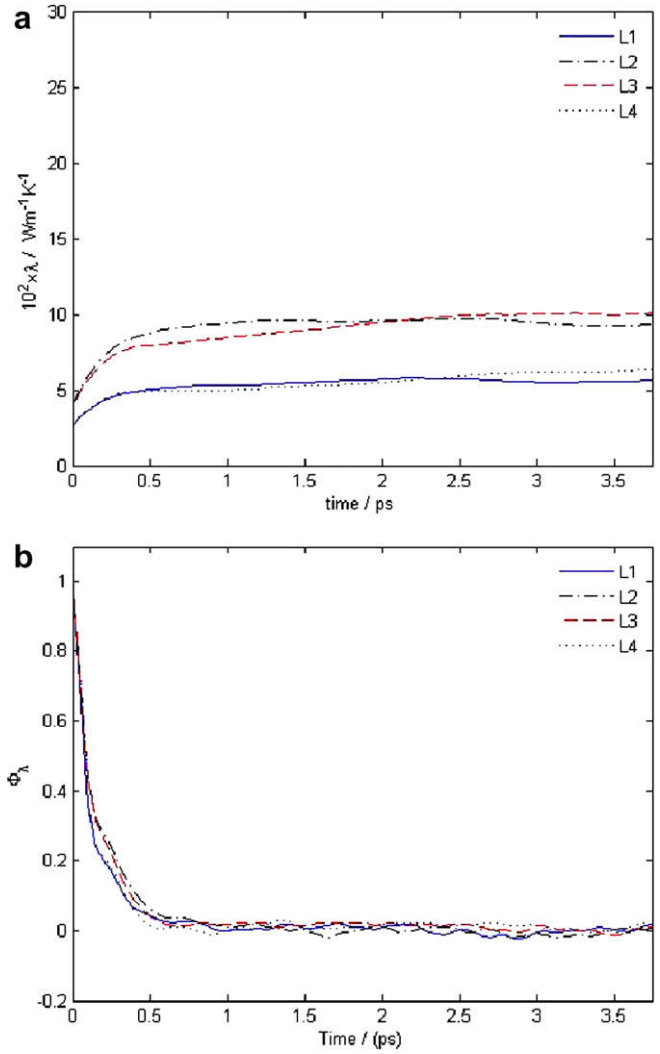

Fig. 10. Thermal conductivity across a 7.9σ-wide channel at 120 K in (a) integral diagrams (b) ACF diagrams. L1 and L4 layers are adjacent to the walls, L2 and L3 layers are in the midplane of the channel.

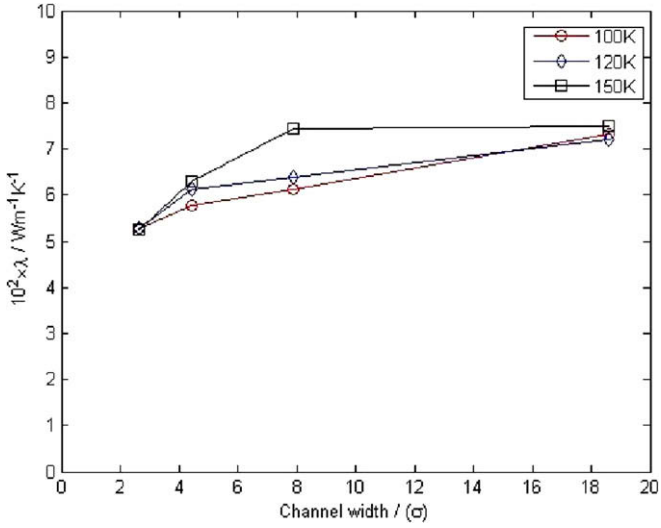

Fig. 11. Estimation of thermal conductivity at 100, 120 and 150 K, for channel widths ranging from 2.65 to 18.58σ (lines are used only as a guide to the eye).

We believe that these effects (due primarily to the existence of the two solid/liquid interfaces) are important characteristics of flows in nanochannels and should be taken into account in the design of nanofluidic devices when heat transfer is significant.

We performed also simulations using three-layer fcc walls. In general, same results were obtained for diffusion coefficients and thermal conductivity. Shear viscosity, as a total average value for each channel, was not significantly affected by the number of wall atomic layers. However, in the case of three-layer walls, near the walls shear viscosity has smaller value (greater values near the channel centerline) compared to the values obtained for the two-layer walls.

5. Conclusions

We have presented a molecular dynamics study of planar Poiseuille nanoflow of liquid argon between krypton walls for channel widths, h, in the range 2.65σ–18.58σ.

Diffusivity is isotropic in planes parallel to the walls, i.e., D_x and D_y are practically the same (x is the direction along the flow and y the spanwise direction, i.e., normal to flow direction and parallel to the walls). On the contrary, in the z-direction (normal to the walls) the diffusion coefficient D_z is significantly smaller than D_x and D_y in the narrow channels $h = 2.65\sigma$ and $h = 4.42\sigma$. The ratio of D_z/D_x (or, similar ly, D_z/D_y) increases as the channel width increases and reaches unity, i.e. isotropic diffusion for $h = 18.58\sigma$. The calculation of the diffusion coefficients in distinct layers parallel to walls reveal that diffusion is higher in layers close to the center of the channel and decreases for the layers adjacent to the walls. This behavior is attributed to the fact that these layers "feel" the presence of walls in contrast to the central layers that are surrounded only by fluid atoms and diffusion is not inhibited by the presence of the solid atoms. As the channel width increases bulk-like behavior is approached close to the centerline. The diffusion coefficient increases when the system temperature increases as the atomic mobility increases at elevated temperatures.

Shear viscosity values are affected by the channel width. The smaller the channel width the larger its value. However, for $h \approx 8\sigma$, η_s attains its bulk value. Across the channel, shear viscosity profiles are nearly uniform with only a slight decrease near the walls. Shear viscosity is not significantly affected by the solid/fluid interaction. At 100 and 120 K thermal conductivity, as an average total value for the whole channel, increases slightly as channel width rises and reaches its bulk value at $h = 20\sigma$. At 150 K, thermal conductivity attains its bulk value for liquid argon at $h \approx 8\sigma$ and retains it as h increases. Thermal conductivity calculated in layers, i.e., profiles across the channel reveal that the layers close to the channel centerline conduct the heat produced by the flow at a higher rate compared to the layers adjacent to the walls, i.e., thermal conductivity attains higher values as we approach the center of the channel.

The results show that transport properties exhibit a significantly different behavior than that of the bulk fluid below a critical channel width which in our system seems to be located in the region 8–20σ. The existence of this critical width is attributed to the interaction of the fluid with the walls since at smaller channel widths the effect of the difference of interactions of the walls on the fluid extends practically to the whole range of the fluid modifying considerably its properties in comparison to the bulk. As the channel width increases there is an increasing percentage of fluid atoms that are located out of the wall range and, as a result, the fluid atoms attain bulk-like behavior. The size of the characteristic width may depend on the type of wall/fluid materials due to the different kind of atomistic interactions.

Acknowledgements

This research project, PENED-uth-3337C, is co-financed by E.U.-European Social Fund (75%) and the Greek Ministry of Development-GSRT (25%).

References

[1] D. Frenkel, B. Smit, Understanding Molecular Simulation, Academic Press, 1996.
[2] D.C. Rapaport, The Art of Molecular Dynamics Simulation, Cambridge University Press, 1995.
[3] G.E. Karniadakis, A. Beskok, N. Aluru, Microflows: Fundamentals and Simulation, Springer, 2002.
[4] K. Binder, J. Horbach, W. Kob, W. Paul, F. Varnik, Molecular dynamics simulations, Journal of Physics: Condensed Matter 16 (2004) 429–453.
[5] J. Koplik, J.R. Banavar, J.F. Willemsen, Molecular dynamics of fluid flow at solid surfaces, Physics of Fluids A 1 (5) (1989) 781–794.
[6] U. Heinbuch, J. Fischer, Liquid flow in pores: slip, no-slip, or multi layer sticking, Physical Review A 40 (2) (1989) 1144–1146.
[7] K.P. Travis, B.D. Todd, D.J. Evans, Departure from Navier-Stokes hydrodynamics in confined liquids, Physical Review E 55 (4) (1997) 4288–4295.
[8] K.P. Travis, K.E. Gubbins, Poiseuille flow of Lennard–Jones fluids in narrow slit pores, Journal of Chemical Physics 112 (4) (2000) 1984–1994.
[9] J. Delhommele, D.J. Evans, Configurational temperature profile in confined liquids. I. Atomic fluid, Journal of Chemical Physics 114 (14) (2001) 6229–6235.
[10] J. Delhommele, D.J. Evans, Configurational temperature profile in confined liquids. II. Molecular fluids, Journal of Chemical Physics 114 (14) (2001) 6236–6241.
[11] M. Wang, J. Liu, S. Chen, Similarity of electroosmotic flows in nanochannels, Molecular Simulation 33 (3) (2007) 239–244.
[12] M. Wang, J. Liu, S. Chen, Electric potential distribution in nanoscale electroosmosis: from molecules to continuum, Molecular Simulation 34 (5) (2008) 509–514.
[13] I. Bitsanis, J.J. Magda, M. Tirell, H.T. Davis, Molecular dynamics of flow in micropores, Journal of Chemical Physics 87 (3) (1987) 1733–1750.
[14] S. Murad, P. Ravi, J.G. Powles, A computer simulation study of fluids in model slit, tubular, and cubic micropores, Journal of Chemical Physics 98 (12) (1993) 9771–9781.
[15] I. Bitsanis, T.K. Vanderlick, M. Tirell, H.T. Davis, A tractable molecular theory of flow in strongly inhomogeneous fluids, Journal of Chemical Physics 89 (5) (1988) 1733–1750.
[16] Y.Z. Hu, H. Wang, Y. Guo, L.Q. Zheng, Simulation of lubricant rheology in thin film lubrication part I: simulation of Poiseuille flow, Wear 196 (1996) 243–248.
[17] D.J. Evans, Thermal conductivity of the Lennard–Jones fluid, Physical Review A 34 (2) (1986) 1449–1453.
[18] S. Murad, P. Ravi, J.G. Powles, Anisotropic thermal conductivity of a fluid in a system of microscopic slit pores, Physical Review E 48 (5) (1993) 4110–4412.
[19] Q.-X. Liu, P.X. Jiang, H. Xiang, Molecular dynamics study of the thermal conductivity of nanoscale argon films, Molecular Simulation 32 (8) (2006) 645–649.
[20] Y. Yonetani, K. Kinugawa, Centroid molecular dynamics approach to the transport properties of liquid para-hydrogen over the wide temperature range, Journal of Chemical Physics 120 (22) (2004) 10624–10633.
[21] F. Sofos, T. Karakasidis, A. Liakopoulos, Nano-channel Poiseuille flow by non-equilibrium molecular dynamics: effect of channel width, temperature and external forces, submitted for publication.
[22] N.V. Priezjev, Effect of surface roughness on rate-dependent slip in simple fluids, Journal of Chemical Physics 127 (2007) 144708.
[23] T.M. Galea, P. Attard, Molecular dynamics study of the effect of atomic roughness on the slip length at the fluid–solid boundary during shear flow, Langmuir 20 (2004) 3477–3482.
[24] G. Mo, F. Rosenberger, Molecular dynamics simulation of flow in two-dimensional channel with atomically rough walls, Physical Review A 42 (1990) 4688–4692.
[25] B.Y. Cao, M. Chen, Z.Y. Guo, Liquid flow in surface-nanostructured channels studied by molecular dynamics simulation, Physical Review E 74 (2006) 066311.
[26] D. Kim, E. Darve, Molecular dynamics simulation of electro-osmotic flows in rough wall nanochannels, Physical Review E 73 (2006) 051203.
[27] A. Jabbardeh, J.D. Atkinson, R.I. Tarner, Effect of the wall roughness on slip and rheological properties of hexadecane in molecular dynamics simulation of Couette shear flow between two sinusoidal walls, Physical Review E 61 (1) (2000) 690–699.
[28] S.Y. Liem, D. Brown, J.H.R. Clarke, Investigation of the homogeneous-shear non-equilibrium-molecular-dynamics method, Physical Review A 45 (6) (1992) 3706–3713.
[29] D.J. Evans, B.L. Holian, The Nosé–Hoover thermostat, Journal of Chemical Physics 83 (8) (1985) 4069–4074.
[30] B.L. Holian, A.F. Voter, Thermostatted molecular dynamics: how to avoid the Toda demon hidden in Nosé–Hoover dynamics, Physical Review E 52 (3) (1995) 2338–2347.
[31] G.A. Fernandez, J. Vrabec, H. Hasse, A molecular simulation study of shear and bulk viscosity and thermal conductivity of simple real fluids, Fluid Phase Equilibria 221 (2004) 157–163.
[32] B.D. Todd, D.J. Evans, P.J. Daivis, Pressure tensor for inhomogeneous fluids, Physical Review E 52 (2) (1995) 1627–1638.
[33] J.L. Hurst, J.T. Wen, Computation of shear viscosity: a systems approach, American Control Conference, Portland, OR, USA, 2005, pp. 2028–2033.
[34] S.A. Somers, H.T. Davis, Microscopic dynamics of fluids confined between smooth and atomically structured solid surfaces, Journal of Chemical Physics 96 (7) (1991) 5389–5407.
[35] C. Bouzigues, P. Tabeling, Study of liquid flows over solid surfaces by particle nanovelocimetry, Bulletin of the APS 52 (17) (2007) 101.
[36] H.L. Song, K.P. Dong, B.K. Dae, Molecular dynamics simulations for transport coefficients of liquid argon: new approaches, Bulletin of the Korean Chemistry Society 24 (2) (2003) 178–182.